

Article

Hydrogen Release and Uptake of MgH₂ Modified by Ti₃CN MXene

Xiantun Huang ^{1,†}, Chenglin Lu ^{2,†}, Yun Li ^{3,*}, Haimei Tang ², Xingqing Duan ², Kuikui Wang ⁴
and Haizhen Liu ^{2,5,*} ¹ Department of Materials Science and Engineering, Baise University, Baise 533000, China² Guangxi Novel Battery Materials Research Center of Engineering Technology, Guangxi Colleges and Universities Key Laboratory of Blue Energy and Systems Integration, School of Physical Science and Technology, Guangxi University, Nanning 530004, China³ School of Mechanical and Electrical Engineering, Quzhou College of Technology, Quzhou 324000, China⁴ College of Materials Science and Engineering, Qingdao University, Qingdao 266071, China; kkwang@qdu.edu.cn⁵ Key Laboratory of Advanced Energy Materials Chemistry (Ministry of Education), Nankai University, Tianjin 300071, China

* Correspondence: shanxiliyun2006@163.com (Y.L.); liuhz@gxu.edu.cn (H.L.)

† These authors contribute equally to this work.

Abstract: MgH₂ has a high hydrogen content of 7.6 wt% and possesses good reversibility under normal conditions. However, pristine MgH₂ requires a high temperature above 300 °C to release hydrogen, with very slow kinetics. In this work, we utilized Ti₃CN MXene to reduce the operating temperature and enhance the kinetics of MgH₂. The initial temperature of MgH₂ decomposition can be lowered from 322 °C for pristine MgH₂ to 214 °C through the employment of Ti₃CN. The desorbed MgH₂ + 7.5 wt% Ti₃CN can start absorption at room temperature, while the desorbed pristine MgH₂ can only start absorption at 120 °C. The employment of Ti₃CN can significantly improve the hydrogen release kinetics of MgH₂, with the desorption activation energy decreasing from 121 to 80 kJ mol⁻¹. Regarding thermodynamics, the desorption enthalpy changes of MgH₂ and MgH₂ + 7.5 wt% Ti₃CN were 79.3 and 78.8 kJ mol⁻¹, respectively. This indicates that the employment of Ti₃CN does not alter the thermal stability of MgH₂. Phase evolution studies through the use of X-ray diffraction and electron diffraction both confirm that Ti₃CN remains stable during the hydrogen release and uptake process of the composite. This work will help understand the impact of a transition metal carbonitride on the hydrogen storage of MgH₂.

Keywords: hydrogen storage materials; magnesium hydride; transition metal carbonitride; 2D materials; layered materials



Citation: Huang, X.; Lu, C.; Li, Y.; Tang, H.; Duan, X.; Wang, K.; Liu, H. Hydrogen Release and Uptake of MgH₂ Modified by Ti₃CN MXene. *Inorganics* **2023**, *11*, 243. <https://doi.org/10.3390/inorganics11060243>

Academic Editors: Craig Buckley, Mark Paskevicius, Torben R. Jensen and Terry Humphries

Received: 29 April 2023

Revised: 27 May 2023

Accepted: 2 June 2023

Published: 5 June 2023



Copyright: © 2023 by the authors. Licensee MDPI, Basel, Switzerland. This article is an open access article distributed under the terms and conditions of the Creative Commons Attribution (CC BY) license (<https://creativecommons.org/licenses/by/4.0/>).

1. Introduction

Hydrogen energy is acknowledged as an ideal strategy to solve energy shortages and environmental pollution issues. However, hydrogen under ambient conditions is a gas of low density (0.089 kg m⁻³) [1]. In addition, it is flammable and combustible with a wide explosion limit of 4–75 vol%. Therefore, the safe and compact storage of hydrogen is an important issue when utilizing hydrogen energy on a large scale [2–4].

Solid-state hydrogen storage, with the hydrogen bonded in a hydrogen storage material, is a good method to store hydrogen since it has a very large capacity (>50 kg m⁻³). In addition, the method is safe since it can be operated under low hydrogen pressure (generally <5 MPa). Construction of high-performance materials for hydrogen storage is the key issue in developing a solid-state hydrogen storage system [5–11].

MgH₂ has attracted extensive attention as a material for hydrogen storage due to its large capacity of 7.6 wt% and the ability to reversibly store hydrogen [12–14]. In

addition, there is an abundant resource of Mg on Earth, which makes large-scale application possible. However, MgH₂ with high thermal stability requires a high temperature to desorb hydrogen. Moreover, the hydrogen sorption process is very slow for MgH₂ when the temperature is not high enough. These two drawbacks have severely limited the practical application of MgH₂. Constructing nanoscale Mg-based materials [12,15–20], alloying Mg with other metals [8,21–24], or introducing additives [25–38] are the commonly utilized strategies to modify the hydrogen sorption properties of MgH₂.

In the past decade, MXenes (transition metal carbides/nitrides with layered structures) have received much attention in catalysis, energy storage, and conversion. MXene has also been demonstrated to show the positive impact on MgH₂ [35,39–47]. In 2016, Liu et al. [47] first reported the enhancing impact of Ti₃C₂ MXene on MgH₂. It was shown that the employment of 7 wt% Ti₃C₂ can reduce the starting hydrogen desorption temperature of MgH₂ to 180 °C. Li et al. [44] used Ti₂C MXene to reduce the temperature of MgH₂ by 37 °C. It was suggested that the Ti elements with multivalences will enhance the electron transfer during hydrogen sorption. Lu et al. [31] showed that V₂C MXene can tailor both the kinetics and thermodynamics of MgH₂. Liu et al. [40] demonstrated that the hybrid of Ti₃C₂ and V₂C MXenes exhibits a synergistic impact on MgH₂. The starting temperature of the hydrogen release of MgH₂–Ti₃C₂/V₂C can be reduced by 140 °C. Bimetallic MXene which contains two transition metals also has a good enhancing impact on MgH₂. For example, Shen et al. [46] reported that MgH₂ + 10 wt% (Ti_{0.5}V_{0.5})₃C₂ can start desorption at 196 °C. Wang et al. [42] displayed that NbTiC MXene reduces the starting hydrogen desorption temperature of MgH₂ to 195 °C. It has been supposed by many researchers that the unique layered structures and the active transition metals contained within both contribute to the enhanced hydrogen storage properties of MgH₂ [40,42–44,46,47].

Based on the above introduction, MXene materials have shown excellent enhancing influence on MgH₂. However, the studies mainly focus on carbides. The impact of transition metal nitrides or carbonitrides on MgH₂ is not clear currently. In this work, we first synthesized a layered transition metal carbonitride (Ti₃CN MXene) and then used it to modify the hydrogen sorption properties of MgH₂. The hydrogen release and uptake kinetics and thermodynamics of MgH₂ modified by Ti₃CN MXene will be investigated. Microstructures will be studied to reveal the role of Ti₃CN MXene in modifying MgH₂.

2. Results

Ti₃CN MXene was synthesized by the exfoliation of Ti₃AlCN MAX (hexagonal layered transition metal carbides and nitrides). A hydrofluoric acid solution was used to remove the Al layers from Ti₃AlCN to synthesize the layered Ti₃CN MXene. Figure 1a shows the XRD spectrum of Ti₃AlCN MAX and Ti₃CN MXene. The diffraction peak of the (002) crystalline plane shifting to a lower angle indicates the exfoliation of Ti₃AlCN MAX to form the layered Ti₃CN MXene. The SEM picture in Figure 1b indicates that Ti₃CN MXene has a layered structure. In Figure 1c, the elemental mappings show that the Ti, C, and N elements are all distributed uniformly in the material. Some traces of the Al element were also observed in the material. The above characterizations indicate the successful synthesis of the layered Ti₃CN MXene.

The Ti₃CN MXene was mixed with MgH₂ by ball milling to obtain MgH₂ + *m* wt% Ti₃CN (*m* = 0, 5, 7.5, 10) composites. Figure 2a shows the hydrogen release curves of the MgH₂ + *m* wt% Ti₃CN (*m* = 0, 5, 7.5, 10) composites when the temperature was increased from room temperature (RT) to about 400 °C at 2 °C min^{−1}. The as-milled MgH₂ without additive starts desorbing hydrogen at 322 °C and could offer a capacity of 7.0 wt% when the temperature reached 400 °C. Excitingly, the addition of Ti₃CN can significantly lower the starting temperature of MgH₂ desorption to 214 °C. This means a reduction of 108 °C in the starting temperature. The 7.5 wt% Ti₃CN-doped MgH₂ has a slightly lower hydrogen desorption temperature than the 5 wt% Ti₃CN-doped MgH₂. However, further increasing the Ti₃CN content to 10 wt% does not further reduce the temperature of MgH₂ but will slightly reduce the capacity of the composite. Considering achieving both low temperature

and high capacity, the MgH_2 with the addition of 7.5 wt% of Ti_3CN was selected for further absorption studies. Figure 2b shows the hydrogen absorption curves of the desorbed $\text{MgH}_2 + 7.5 \text{ wt}\% \text{ Ti}_3\text{CN}$ composite and the pristine MgH_2 at 4 MPa H_2 . During absorption, the temperature was increased from RT to 400 °C at 2 °C min^{-1} . The desorbed MgH_2 starts to absorb hydrogen at about 120 °C and could absorb 7.4 wt% H_2 after the temperature was ramped to 400 °C. It is exciting that the desorbed $\text{MgH}_2 + 7.5 \text{ wt}\% \text{ Ti}_3\text{CN}$ sample can start to absorb hydrogen at RT and absorb 7.0 wt% H_2 at 400 °C. Therefore, Ti_3CN MXene can significantly improve the non-isothermal hydrogen desorption and absorption performance of MgH_2 .

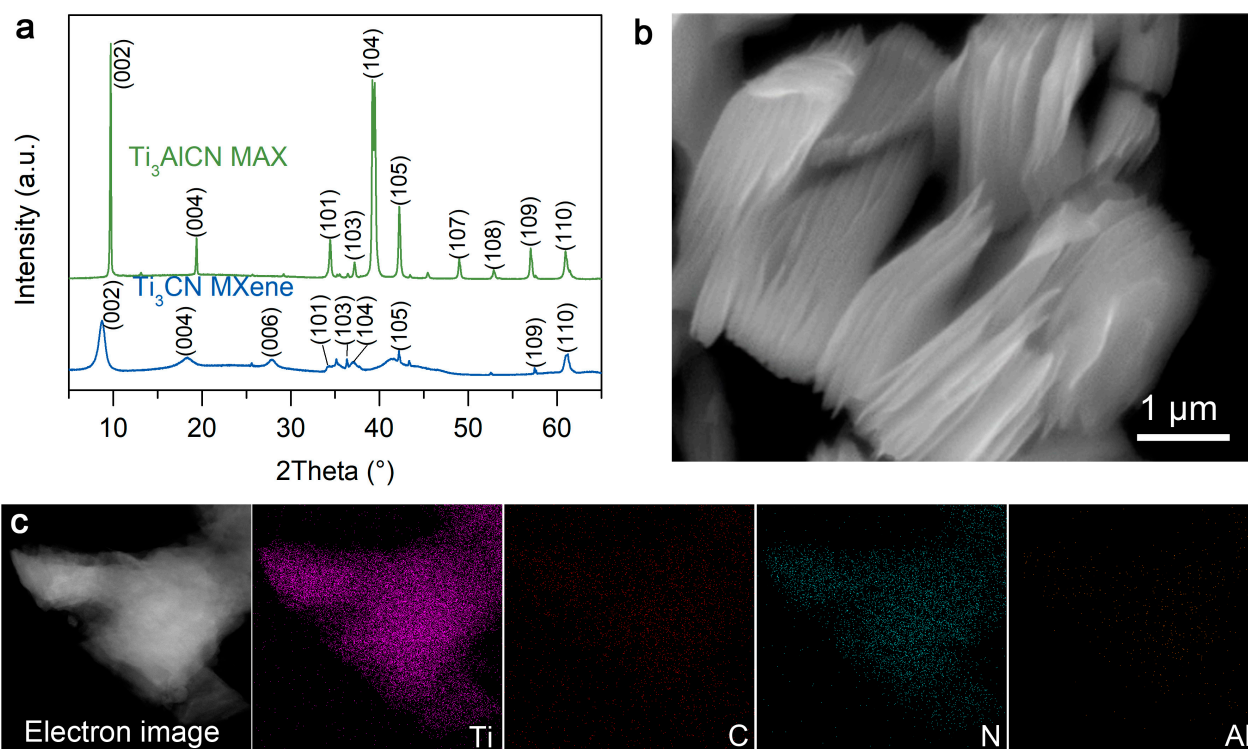


Figure 1. (a) XRD spectrum of Ti_3AlCN and Ti_3CN . (b) SEM image of Ti_3CN . (c) EDS elemental distributions of Ti_3CN .

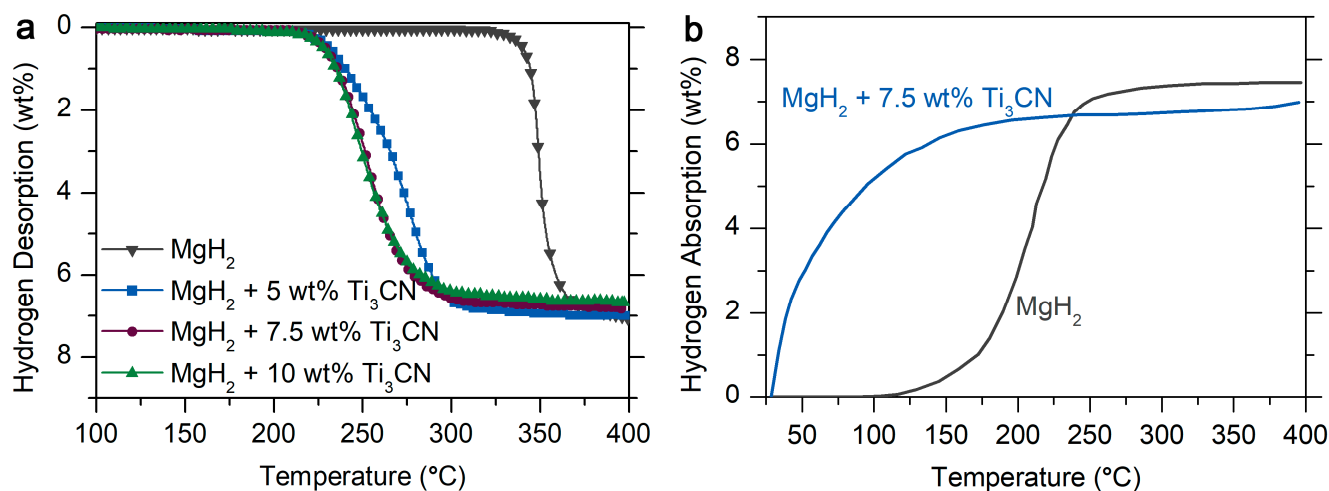


Figure 2. (a) Hydrogen release curves of $\text{MgH}_2 + m \text{ wt}\% \text{ Ti}_3\text{CN}$ ($m = 0, 5, 7.5, 10$) with the temperature rising from RT to 400 °C at 2 °C min^{-1} . (b) Hydrogen uptake curves of MgH_2 and $\text{MgH}_2 + 7.5 \text{ wt}\% \text{ Ti}_3\text{CN}$ at 6 MPa H_2 with the same temperature program as (a).

The hydrogen release kinetics of MgH_2 and $\text{MgH}_2 + 7.5 \text{ wt\% Ti}_3\text{CN}$ were studied by testing the isothermal hydrogen desorption curves, as shown in Figure 3a,d, respectively. The MgH_2 without an additive can achieve fast kinetics only at a temperature higher than 350°C . However, the $\text{MgH}_2 + 7.5 \text{ wt\% Ti}_3\text{CN}$ composite has fast hydrogen desorption kinetics even at a lower temperature below 300°C . At a constant temperature of 300°C , $\text{MgH}_2 + 7.5 \text{ wt\% Ti}_3\text{CN}$ can desorb 6.6 wt\% H_2 within 10 min and 6.9 wt\% within 60 min. Therefore, the hydrogen release kinetics were greatly improved by Ti_3CN addition. The curves in Figure 3a,d were further studied by the Johnson–Mehl–Avrami (JMA) equation and the Arrhenius equation. The JMA equation is:

$$\ln[-\ln(1 - \alpha)] = n \ln k + n \ln t, \quad (1)$$

where α refers to the extent of the reaction; n represents the Avrami index; t is the time; k stands for the reaction rate constant. The isothermal hydrogen desorption curves were converted to JMA plots ($\ln[-\ln(1 - \alpha)]$ vs. $\ln t$) as shown in Figure 3b,e. Then, linear fitting was performed to obtain the n and $n \ln k$ from the slopes and the intercepts. The $n \ln k$ values were then plotted vs. $1000/T$ based on the Arrhenius equation, which is:

$$\ln k = -E_a/RT + \ln A, \quad (2)$$

where E_a refers to the activation energy; R represents the universal gas constant; and A stands for a constant. The Arrhenius plots ($\ln k$ vs. $1000/T$) are shown in Figure 3c,f. Then, linear fitting was performed to obtain the values of E_a from the slope. The desorption activation energy for $\text{MgH}_2 + 7.5 \text{ wt\% Ti}_3\text{CN}$ was estimated to be 80 kJ mol^{-1} , which is much lower compared to MgH_2 without an additive (121 kJ mol^{-1}). This indicates that Ti_3CN improved the hydrogen release kinetics of MgH_2 .

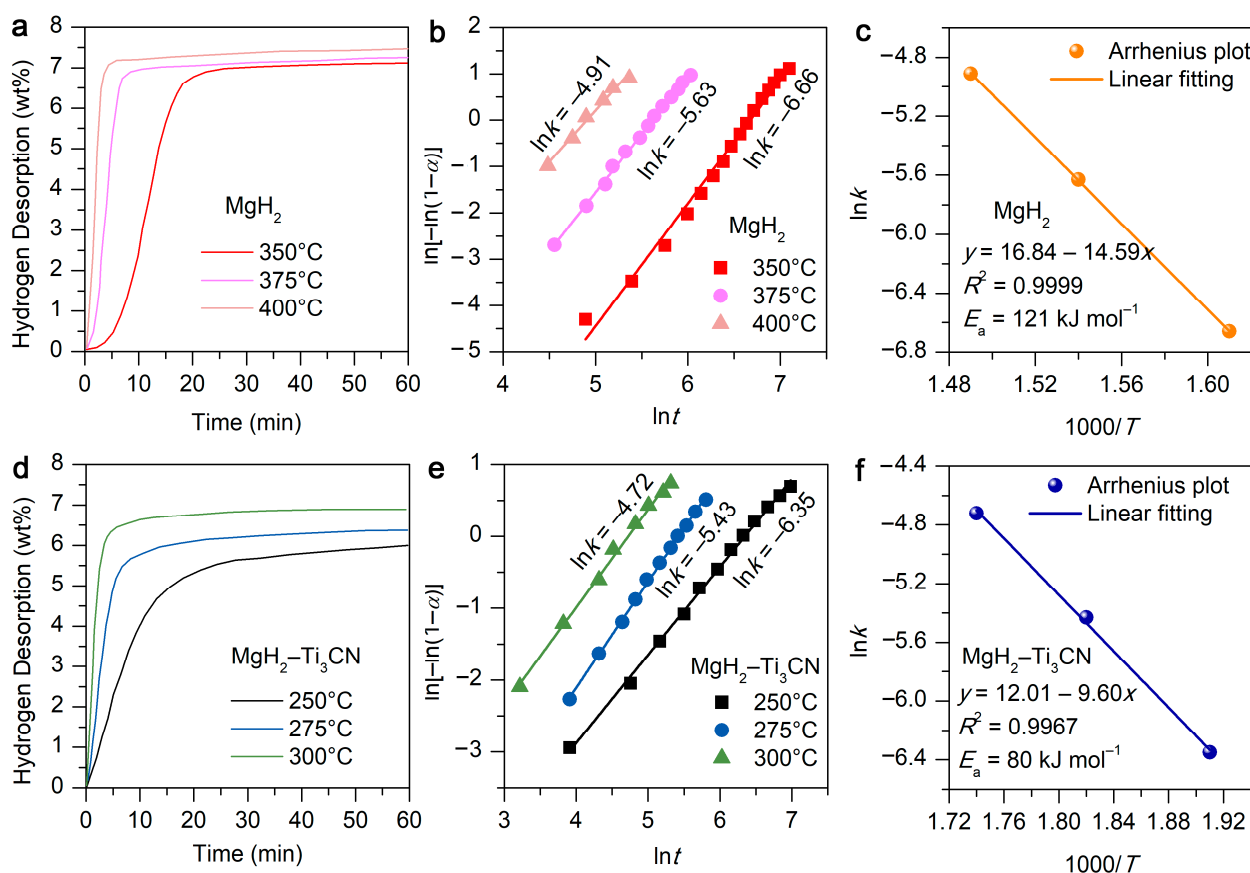


Figure 3. Hydrogen release curves at various temperatures (a,d), JMA plots (b,e), and Arrhenius plots (c,f) of MgH_2 without addition (upper) and $\text{MgH}_2 + 7.5 \text{ wt\% Ti}_3\text{CN}$ (down).

The thermodynamics of MgH_2 were further studied by testing the pressure–concentration isotherms (PCT) and using the van't Hoff equation written as:

$$\ln(p/p_0) = -\Delta H/RT + \Delta S/R, \quad (3)$$

where p refers to the plateau hydrogen pressure; p_0 stands for the standard atmosphere pressure; ΔH represents the enthalpy change of the reaction; and ΔS represents the entropy changes of the reaction. Figure 4a,c shows the hydrogen desorption PCT curves of the two samples at various temperatures. From the PCT curves, the plateau hydrogen pressures (p) can be obtained. Then, the van't Hoff plots ($\ln(p/p_0)$ vs. $1000/RT$) can be made (Figure 4b,d). The slopes of the linear fitting lines give the values of ΔH . The enthalpy change for the hydrogen release reaction of $\text{MgH}_2 + 7.5 \text{ wt\% Ti}_3\text{CN}$ was estimated to be 78.8 kJ mol^{-1} , which is very equal to that of MgH_2 without an additive (79.3 kJ mol^{-1}). Therefore, Ti_3CN addition does not alter the thermodynamics of MgH_2 .

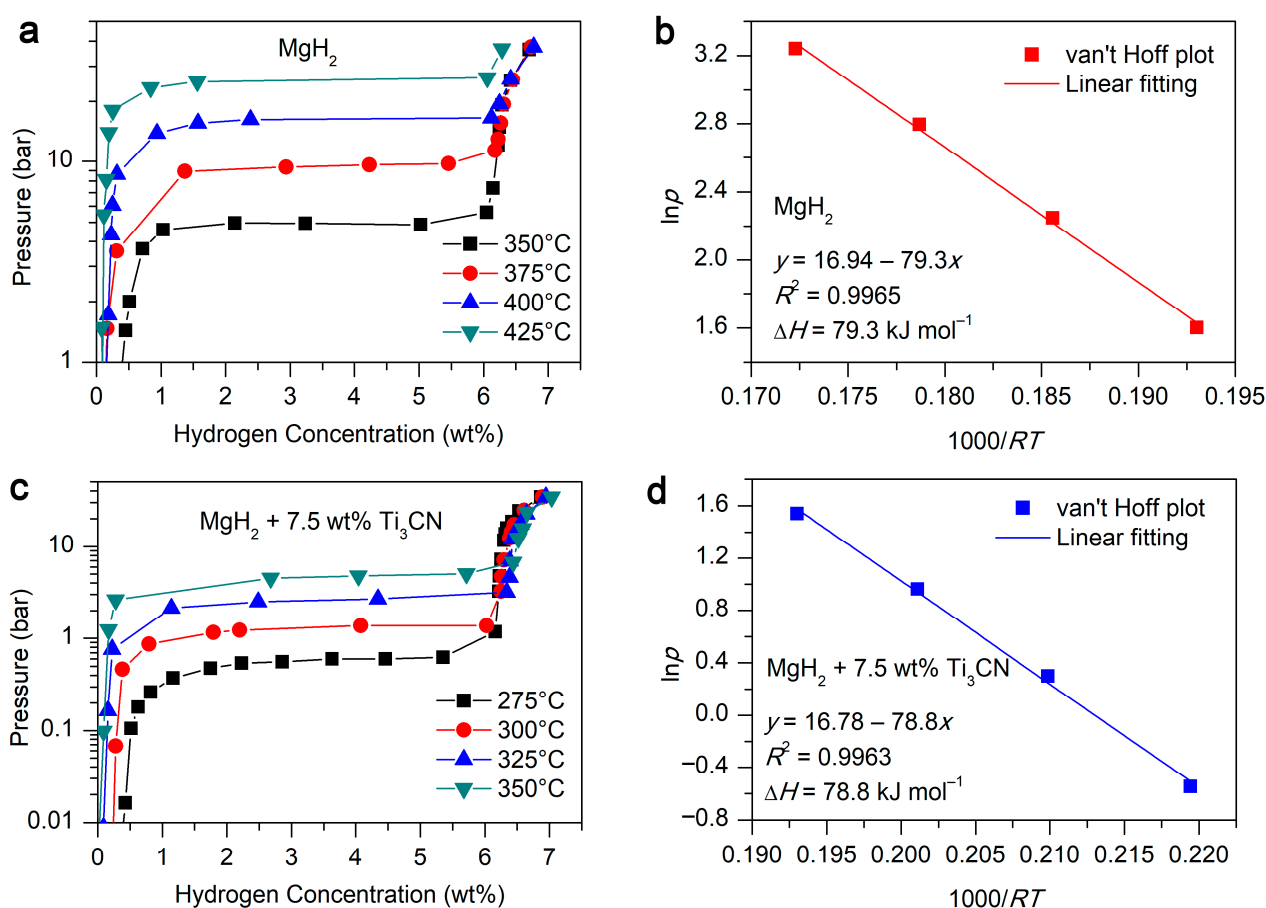


Figure 4. Hydrogen desorption PCT curves (a,c) and van't Hoff plots (b,d) of MgH_2 without addition (upper) and $\text{MgH}_2 + 7.5 \text{ wt\% Ti}_3\text{CN}$ (down).

To reveal the role of Ti_3CN MXene in tailoring the hydrogen storage of MgH_2 , the structures of $\text{MgH}_2 + 7.5 \text{ wt\% Ti}_3\text{CN}$ in different states were studied by X-ray diffraction (XRD). Figure 5b–d shows the XRD profiles of $\text{MgH}_2 + 7.5 \text{ wt\% Ti}_3\text{CN}$ at different stages, with the as-synthesized Ti_3CN MXene for reference (Figure 5a). After ball milling (Figure 5b), MgH_2 and Ti_3CN were observed in the sample, suggesting that it is a physical mixture of the starting materials. After hydrogen desorption (Figure 5c), MgH_2 decomposes and Mg forms. Ti_3CN is still observed in the desorbed sample, which indicates that Ti_3CN does not react with other components and stays stable in the sample. It should be noted that MgO is observed in the sample, which may be due to the partial oxidation of MgH_2/Mg during sample transfer or testing. After hydrogen absorption (Figure 5d), MgH_2 is fully recovered

and Ti_3CN is still observed in the sample. From the above structure evolution studies, it can be seen that Ti_3CN stays stable during the hydrogen release and uptake process. Therefore, Ti_3CN mainly plays the role of an efficient catalyst for the hydrogen release and uptake of MgH_2 . This is consistent with the results in Figure 4 in that the thermodynamics of MgH_2 is not altered by the addition of Ti_3CN .

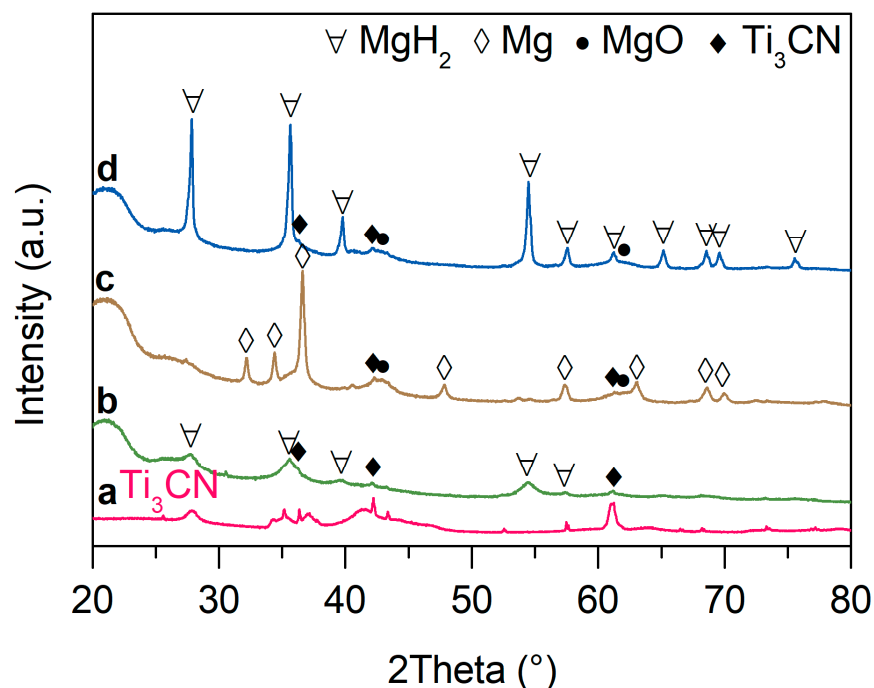


Figure 5. XRD profiles of Ti_3CN MXene (a) and $\text{MgH}_2 + 7.5 \text{ wt}\% \text{Ti}_3\text{CN}$ after ball milling (b), after hydrogen desorption (c), and after hydrogen absorption (d).

The microstructures of the $\text{MgH}_2 + 7.5 \text{ wt}\% \text{Ti}_3\text{CN}$ composite after rehydrogenation were further studied by SEM, TEM, EDS, and SAED methods. Figure 6a shows the SEM image of the composite, which displays that the particles of the composite are of several microns. Figure 6b shows the EDS elemental mappings of the composite. The Mg, Ti, C, and N elements are all distributed very uniformly in the composite. Figure 6c shows the TEM image of the composite with its SAED pattern shown in Figure 6d. In the SAED pattern, MgH_2 , Mg, and Ti_3CN are observed. These three components are also observed in the HRTEM images in Figure 6e–i. The presence of Ti_3CN is consistent with the XRD results in Figure 5d, which again suggests that Ti_3CN mainly plays the role of an efficient catalyst for MgH_2 . It is interesting that Mg is detected in the rehydrogenated composite, which is different from Figure 5d. In Figure 5d, Mg is not observed in the XRD pattern. This indicates that the high-energy electron beam may have stimulated the partial decomposition of the Ti_3CN -modified MgH_2 . It should be also noted that only those MgH_2 particles that are contacting with Ti_3CN can be stimulated to decompose by the high-energy electron beam, as shown in regions 1 and 3 of Figure 6e. In region 4 of Figure 6e, MgH_2 without contacting with Ti_3CN is not decomposed. Therefore, Ti_3CN indeed is an excellent catalyst for MgH_2 .

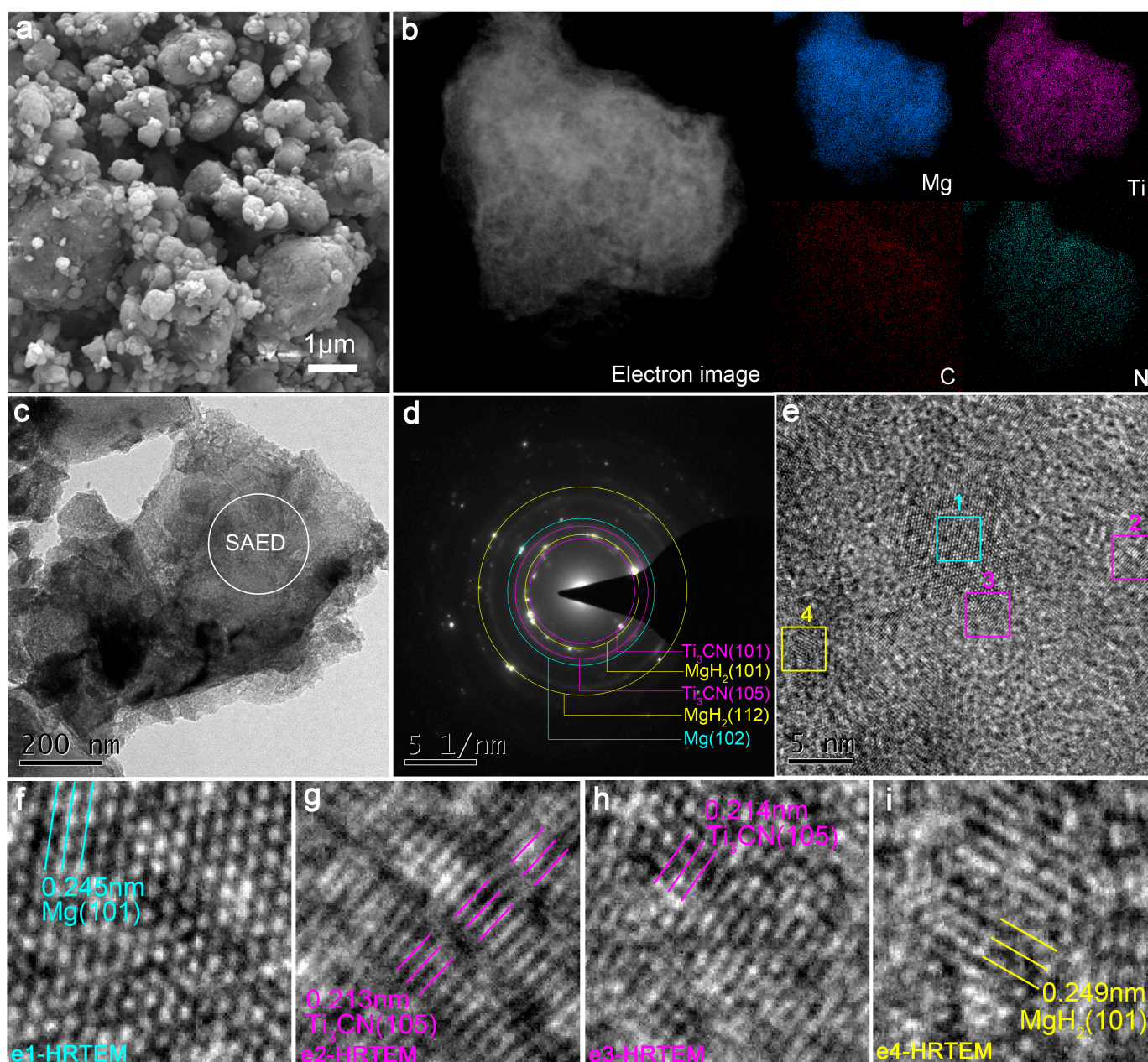


Figure 6. SEM image (a), EDS elemental mappings (b), TEM image (c), SAED pattern (d), and HRTEM image (e–i) of the $\text{MgH}_2 + 7.5 \text{ wt\% Ti}_3\text{CN}$ composite after rehydrogenation.

3. Discussion

From the above results, it can be said that Ti_3CN MXene can greatly enhance the hydrogen sorption kinetics of MgH_2 . The addition of Ti_3CN can lower the initial hydrogen release temperature of MgH_2 from 322 °C to 214 °C, with a reduction of 108 °C. Moreover, the desorbed MgH_2 starts to absorb hydrogen at about 120 °C, while the desorbed $\text{MgH}_2 + 7.5 \text{ wt\% Ti}_3\text{CN}$ sample can start to absorb hydrogen at RT. The $\text{MgH}_2 + 7.5 \text{ wt\% Ti}_3\text{CN}$ has a desorption activation energy of 80 kJ mol^{-1} , which is significantly lower than that of pristine MgH_2 (121 kJ mol^{-1}).

However, it seems that Ti_3CN does not alter the thermodynamics of MgH_2 . Many published papers have demonstrated that MXene materials such as Ti_3C_2 [41,45,47], Ti_2C [44], NbTiC [42], $(\text{Ti}_{0.5}\text{V}_{0.5})_3\text{C}_2$ [46], etc., can enhance the hydrogen sorption kinetics of MgH_2 . However, there is barely any work that has reported that MXene materials can reduce the thermal stability of MgH_2 except for V_2C MXene [31]. Therefore, it can be deduced that

most MXene materials do not change the thermodynamics of MgH_2 but mainly alter the kinetics of MgH_2 .

4. Materials and Methods

Ti_3AlCN MAX (500 mesh, 98% purity) was purchased from Laizhou Kaixi Ceramic Co., Ltd., Laizhou, China. MgH_2 (98% purity) was purchased from Langfang Beide Commerce and Trade Co., Ltd., Langfang, China. HF (analytical purity, 40%) was purchased from Aladdin, Shanghai, China. These reagents were used as received without any further treatment.

HF-etching was used to synthesize the layered Ti_3CN MXene. In the experiment, 3 g of Ti_3AlCN MAX was added into a 40 mL HF solution with a concentration of 40%. The solution was then stirred at 30 °C for 18 h followed by centrifugation three times. The rotation speed used for centrifugation was 3500 rpm. After that, the sediment was washed until the pH value of the deionized water used was higher than 6. Then, the sediment was dried in a freeze-dryer for 24 h. After that, Ti_3CN MXene can finally be obtained.

Ti_3CN was then mixed with MgH_2 by ball milling under an argon atmosphere to prepare $\text{MgH}_2 + m \text{ wt}\% \text{ Ti}_3\text{CN}$ ($m = 0, 5, 7.5, 10$) samples at a planetary ball mill (Pulverisette 7, Fritsch, Germany). The as-received MgH_2 and the as-synthesized Ti_3CN were first weighted based on the compositions in a glove box filled with high-purity argon and then placed in a milling jar. Some milling balls were also placed in the milling jar with a ball-to-powder ratio of 40:1. After sealing, the milling jar was transferred to the planetary ball mill. All samples were milled at 400 rpm for 10 h.

An X-ray diffraction (XRD) instrument (Miniflex 600, Rigaku, Japan) was utilized to determine the phase structures. The incident ray was $\text{Cu K}\alpha$ radiation and the scanning speed was 2 °C min^{-1} . A working current of 200 mA and a working voltage of 40 kV were used during the tests. The samples for the XRD test were sealed with transparent tape to prevent the samples from oxidizing during the sample transfer and test. Scanning electron microscopy (SEM, JSM-6510A, JEOL, Japan) was employed to analyze the morphologies. The samples were adhered to conductive tape. The transfer of the samples was carried out carefully to protect the samples from contacting the air. An attached X-ray energy dispersive detector (EDS) was employed to collect the elemental distributions. A transition electronic microscope (TEM, Tecnai G2 F20, FEI, The Netherlands) with a voltage of 200 kV was used to study the microstructures of the samples. Anhydrous acetone was used to disperse the sample on Cu grids.

A Sievert-type apparatus built by the Institute of Metallic Materials, Zhejiang University, Hangzhou, China, was utilized to study the hydrogen release and uptake behavior of the samples. During the non-isothermal hydrogen release tests, the samples were heated gradually from RT to 400 °C at 2 °C min^{-1} from an initial pressure of 10^{-4} MPa. During the non-isothermal hydrogen uptake tests, the temperature program was the same as the isothermal hydrogen release test. At the starting point of the heating program, hydrogen of 6 MPa was charged into the sample holder. During the isothermal hydrogen release tests, the samples were first heated to the target temperature with a hydrogen back pressure of 6 MPa. When the temperature was stabilized, hydrogen gas was rapidly vented to start hydrogen desorption. An automatic Sievert-type apparatus (IMI-Flow, Hiden, UK) was used to collect the PCT curves of the samples.

5. Conclusions

Layered Ti_3CN MXene was successfully synthesized by exfoliation of Ti_3AlCN MAX with HF as the etching solution. The layered Ti_3CN can significantly improve the kinetics of MgH_2 . In particular, $\text{MgH}_2 + 7.5 \text{ wt}\% \text{ Ti}_3\text{CN}$ shows good hydrogen desorption performance, with an initial hydrogen release temperature of 214 °C and a low hydrogen release reaction activation energy of 80 kJ mol^{-1} . Moreover, the desorbed $\text{MgH}_2 + 7.5 \text{ wt}\% \text{ Ti}_3\text{CN}$ can absorb hydrogen at RT, while the desorbed pristine MgH_2 can only start absorption at 120 °C. The layered Ti_3CN barely changes the thermodynamics of MgH_2 since the enthalpy changes of the hydrogen release reactions of MgH_2 and $\text{MgH}_2 + 7.5 \text{ wt}\% \text{ Ti}_3\text{CN}$ are very

close (79.3 and 78.8 kJ mol⁻¹, respectively). Ti₃CN stays stable during the hydrogen release and uptake process of the MgH₂–Ti₃CN composite, which means that Ti₃CN mainly plays the role of an efficient catalyst for MgH₂. This work confirms that transition metal carbonitrides also have a good catalytic impact on the hydrogen release and uptake properties of MgH₂.

Author Contributions: Conceptualization, C.L. and X.H.; methodology, X.D.; validation, H.T.; formal analysis, C.L.; investigation, X.H.; writing—original draft preparation, H.L.; writing—review and editing, Y.L. and K.W.; supervision, H.L.; project administration, H.L.; funding acquisition, Y.L., K.W. and H.L. All authors have read and agreed to the published version of the manuscript.

Funding: This research was funded by the Science and Technology Department of Guangxi Zhuang Autonomous Region, grant number GuiKeAD21238022, the National Natural Science Foundation of China, grant number 52001079, the Quzhou Science and Technology Project, grant number 2022K103, and the open foundation of State Key Laboratory of Featured Metal Materials and Life-cycle Safety for Composite Structures, Guangxi University, grant number 2022GXYSOF16.

Data Availability Statement: The data presented in this study are available from the corresponding author upon request.

Conflicts of Interest: The authors declare no conflict of interest.

References

1. Yang, Z.-X.; Li, X.-G.; Yao, Q.-L.; Lu, Z.-H.; Zhang, N.; Xia, J.; Yang, K.; Wang, Y.-Q.; Zhang, K.; Liu, H.-Z.; et al. 2022 roadmap on hydrogen energy from production to utilizations. *Rare Met.* **2022**, *41*, 3251–3267. [[CrossRef](#)]
2. Schlapbach, L.; Züttel, A. Hydrogen-storage materials for mobile applications. *Nature* **2001**, *414*, 353–358. [[CrossRef](#)] [[PubMed](#)]
3. Berstad, D.; Gardarsdottir, S.; Roussanaly, S.; Voldsund, M.; Ishimoto, Y.; Neksa, P. Liquid hydrogen as prospective energy carrier: A brief review and discussion of underlying assumptions applied in value chain analysis. *Renew. Sust. Energy Rev.* **2022**, *154*, 111772. [[CrossRef](#)]
4. Hassan, I.A.; Ramadan, H.S.; Saleh, M.A.; Hissel, D. Hydrogen storage technologies for stationary and mobile applications: Review, analysis and perspectives. *Renew. Sust. Energy Rev.* **2021**, *149*, 111311. [[CrossRef](#)]
5. Liu, L.; Ilyushechkin, A.; Liang, D.; Cousins, A.; Tian, W.; Chen, C.; Yin, J.; Schoeman, L. Metal Hydride Composite Structures for Improved Heat Transfer and Stability for Hydrogen Storage and Compression Applications. *Inorganics* **2023**, *11*, 181. [[CrossRef](#)]
6. Yao, J.; Wu, Z.; Wang, H.; Yang, F.; Ren, J.; Zhang, Z. Application-oriented hydrolysis reaction system of solid-state hydrogen storage materials for high energy density target: A review. *J. Energy Chem.* **2022**, *74*, 218–238. [[CrossRef](#)]
7. Simanullang, M.; Prost, L. Nanomaterials for on-board solid-state hydrogen storage applications. *Int. J. Hydrogen Energy* **2022**, *47*, 29808–29846. [[CrossRef](#)]
8. Lin, H.J.; Lu, Y.S.; Zhang, L.T.; Liu, H.Z.; Edalati, K.; Révész, Á. Recent advances in metastable alloys for hydrogen storage: A review. *Rare Met.* **2022**, *41*, 1797–1817. [[CrossRef](#)]
9. Zhao, L.; Xu, F.; Zhang, C.; Wang, Z.; Ju, H.; Gao, X.; Zhang, X.; Sun, L.; Liu, Z. Enhanced hydrogen storage of alanates: Recent progress and future perspectives. *Prog. Nat. Sci. Mater. Int.* **2021**, *31*, 165–179. [[CrossRef](#)]
10. Liu, H.; Zhang, L.; Ma, H.; Lu, C.; Luo, H.; Wang, X.; Huang, X.; Lan, Z.; Guo, J. Aluminum hydride for solid-state hydrogen storage: Structure, synthesis, thermodynamics, kinetics, and regeneration. *J. Energy Chem.* **2021**, *52*, 428–440. [[CrossRef](#)]
11. Jiang, W.; Wang, H.; Zhu, M. AlH₃ as a hydrogen storage material: Recent advances, prospects and challenges. *Rare Met.* **2021**, *40*, 3337–3356. [[CrossRef](#)]
12. Sui, Y.; Yuan, Z.; Zhou, D.; Zhai, T.; Li, X.; Feng, D.; Li, Y.; Zhang, Y. Recent progress of nanotechnology in enhancing hydrogen storage performance of magnesium-based materials: A review. *Int. J. Hydrogen Energy* **2022**, *47*, 30546–30566. [[CrossRef](#)]
13. Shang, Y.; Pistidda, C.; Gizer, G.; Klassen, T.; Dornheim, M. Mg-based materials for hydrogen storage. *J. Magnes. Alloy.* **2021**, *9*, 1837–1860. [[CrossRef](#)]
14. Grigorova, E.; Nihitjanova, D.; Tsyntsarski, B.; Stoycheva, I. Investigation of Hydrogen Storage Characteristics of MgH₂ Based Materials with Addition of Ni and Activated Carbon. *Inorganics* **2020**, *8*, 12. [[CrossRef](#)]
15. Ren, L.; Zhu, W.; Zhang, Q.; Lu, C.; Sun, F.; Lin, X.; Zou, J. MgH₂ confinement in MOF-derived N-doped porous carbon nanofibers for enhanced hydrogen storage. *Chem. Eng. J.* **2022**, *434*, 134701. [[CrossRef](#)]
16. Zhang, X.; Liu, Y.; Ren, Z.; Zhang, X.; Hu, J.; Huang, Z.; Lu, Y.; Gao, M.; Pan, H. Realizing 6.7 wt% reversible storage of hydrogen at ambient temperature with non-confined ultrafine magnesium hydrides. *Energy Environ. Sci.* **2021**, *14*, 2302–2313. [[CrossRef](#)]
17. Yan, N.; Lu, X.; Lu, Z.; Yu, H.; Wu, F.; Zheng, J.; Wang, X.; Zhang, L. Enhanced hydrogen storage properties of Mg by the synergistic effect of grain refinement and NiTiO₃ nanoparticles. *J. Magnes. Alloy.* **2022**, *10*, 3542–3552. [[CrossRef](#)]
18. Si, T.-Z.; Zhang, X.-Y.; Feng, J.-J.; Ding, X.-L.; Li, Y.-T. Enhancing hydrogen sorption in MgH₂ by controlling particle size and contact of Ni catalysts. *Rare Met.* **2021**, *40*, 995–1002. [[CrossRef](#)]

19. Le, T.T.; Pistidda, C.; Nguyen, V.H.; Singh, P.; Raizada, P.; Klassen, T.; Dornheim, M. Nanoconfinement effects on hydrogen storage properties of MgH₂ and LiBH₄. *Int. J. Hydrogen Energy* **2021**, *46*, 23723–23736. [[CrossRef](#)]
20. Zhang, X.L.; Liu, Y.F.; Zhang, X.; Hu, J.J.; Gao, M.X.; Pan, H.G. Empowering hydrogen storage performance of MgH₂ by nanoengineering and nanocatalysis. *Mater. Today Nano* **2020**, *9*, 100064. [[CrossRef](#)]
21. Pang, X.; Ran, L.; Chen, Y.A.; Luo, Y.; Pan, F. Enhancing hydrogen storage performance via optimizing Y and Ni element in magnesium alloy. *J. Magnes. Alloy.* **2022**, *10*, 821–835. [[CrossRef](#)]
22. Liu, P.; Lian, J.; Chen, H.; Liu, B.; Zhou, S. In situ formation of Mg₂Ni on magnesium surface via hydrogen activation for improving hydrogen sorption performance. *ACS Appl. Energy Mater.* **2022**, *5*, 6043–6049. [[CrossRef](#)]
23. Ali, N.A.; Ismail, M. Advanced hydrogen storage of the Mg-Na-Al system: A review. *J. Magnes. Alloy.* **2021**, *9*, 1111–1122. [[CrossRef](#)]
24. Yong, H.; Guo, S.; Yuan, Z.; Qi, Y.; Zhao, D.; Zhang, Y. Phase transformation, thermodynamics and kinetics property of Mg₉₀Ce₅RE₅ (RE = La, Ce, Nd) hydrogen storage alloys. *J. Mater. Sci. Technol.* **2020**, *51*, 84–93. [[CrossRef](#)]
25. Tian, G.; Wu, F.; Zhang, H.; Wei, J.; Zhao, H.; Zhang, L. Boosting the hydrogen storage performance of MgH₂ by Vanadium based complex oxides. *J. Phys. Chem. Solids* **2023**, *174*, 111187. [[CrossRef](#)]
26. Lu, Z.Y.; He, J.H.; Song, M.C.; Zhang, Y.; Wu, F.Y.; Zheng, J.G.; Zhang, L.T.; Chen, L.X. Bullet-like vanadium-based MOFs as a highly active catalyst for promoting the hydrogen storage property in MgH₂. *Int. J. Min. Met. Mater.* **2023**, *30*, 44–53. [[CrossRef](#)]
27. Duan, X.-Q.; Li, G.-X.; Zhang, W.-H.; Luo, H.; Tang, H.-M.; Xu, L.; Sheng, P.; Wang, X.-H.; Huang, X.-T.; Huang, C.-K.; et al. Ti₃AlCN MAX for tailoring MgH₂ hydrogen storage material: From performance to mechanism. *Rare Met.* **2023**, in press. [[CrossRef](#)]
28. Yuan, Z.; Li, S.; Wang, K.; Xu, N.; Sun, W.; Sun, L.; Cao, H.; Lin, H.; Zhu, Y.; Zhang, Y. In-situ formed Pt nano-clusters serving as destabilization-catalysis bi-functional additive for MgH₂. *Chem. Eng. J.* **2022**, *435*, 135050. [[CrossRef](#)]
29. Shao, Y.; Gao, H.; Tang, Q.; Liu, Y.; Liu, J.; Zhu, Y.; Zhang, J.; Li, L.; Hu, X.; Ba, Z. Ultra-fine TiO₂ nanoparticles supported on three-dimensionally ordered macroporous structure for improving the hydrogen storage performance of MgH₂. *Appl. Surf. Sci.* **2022**, *585*, 152561. [[CrossRef](#)]
30. Pukazhselvan, D.; Sandhya, K.S.; Ramasamy, D.; Shaula, A.; Bdikin, I.; Fagg, D.P. Active catalytic species generated in situ in zirconia incorporated hydrogen storage material magnesium hydride. *J. Magnes. Alloy.* **2022**, *10*, 786–796. [[CrossRef](#)]
31. Lu, C.; Liu, H.; Xu, L.; Luo, H.; He, S.; Duan, X.; Huang, X.; Wang, X.; Lan, Z.; Guo, J. Two-dimensional vanadium carbide for simultaneously tailoring the hydrogen sorption thermodynamics and kinetics of magnesium hydride. *J. Magnes. Alloy.* **2022**, *10*, 1051–1065. [[CrossRef](#)]
32. Lan, Z.; Fu, H.; Zhao, R.; Liu, H.; Zhou, W.; Ning, H.; Guo, J. Roles of in situ-formed NbN and Nb₂O₅ from N-doped Nb₂C MXene in regulating the re/hydrogenation and cycling performance of magnesium hydride. *Chem. Eng. J.* **2022**, *431*, 133985. [[CrossRef](#)]
33. Dan, L.; Wang, H.; Liu, J.; Ouyang, L.; Zhu, M. H₂ plasma reducing Ni nanoparticles for superior catalysis on hydrogen sorption of MgH₂. *ACS Appl. Energy Mater.* **2022**, *5*, 4976–4984. [[CrossRef](#)]
34. Dai, M.; Lei, G.T.; Zhang, Z.; Li, Z.; Cao, H.J.; Chen, P. Room temperature hydrogen absorption of V₂O₅ catalyzed MgH₂/Mg. *Acta Chim. Sin.* **2022**, *80*, 303–309. [[CrossRef](#)]
35. Bolarin, J.A.; Zou, R.; Li, Z.; Zhang, Z.; Cao, H. MXenes for magnesium-based hydrides: A review. *Appl. Mater. Today* **2022**, *29*, 101570. [[CrossRef](#)]
36. Lu, Z.-Y.; Yu, H.-J.; Lu, X.; Song, M.-C.; Wu, F.-Y.; Zheng, J.-G.; Yuan, Z.-F.; Zhang, L.-T. Two-dimensional vanadium nanosheets as a remarkably effective catalyst for hydrogen storage in MgH₂. *Rare Met.* **2021**, *40*, 3195–3204. [[CrossRef](#)]
37. Liu, X.-S.; Liu, H.-Z.; Qiu, N.; Zhang, Y.-B.; Zhao, G.-Y.; Xu, L.; Lan, Z.-Q.; Guo, J. Cycling hydrogen desorption properties and microstructures of MgH₂-AlH₃-NbF₅ hydrogen storage materials. *Rare Met.* **2021**, *40*, 1003–1007. [[CrossRef](#)]
38. Zhou, C.; Zhang, J.; Bowman, R.C.; Fang, Z.Z. Roles of Ti-Based Catalysts on Magnesium Hydride and Its Hydrogen Storage Properties. *Inorganics* **2021**, *9*, 36. [[CrossRef](#)]
39. Gao, H.; Shi, R.; Liu, Y.; Zhu, Y.; Zhang, J.; Hu, X.; Li, L. Enhanced hydrogen storage performance of magnesium hydride with incompletely etched Ti₃C₂T_x: The nonnegligible role of Al. *Appl. Surf. Sci.* **2022**, *600*, 154140. [[CrossRef](#)]
40. Liu, H.; Lu, C.; Wang, X.; Xu, L.; Huang, X.; Wang, X.; Ning, H.; Lan, Z.; Guo, J. Combinations of V₂C and Ti₃C₂ MXenes for boosting the hydrogen storage performances of MgH₂. *ACS Appl. Mater. Interfaces* **2021**, *13*, 13235–13247. [[CrossRef](#)]
41. Kong, Q.; Zhang, H.; Yuan, Z.; Liu, J.; Li, L.; Fan, Y.; Fan, G.; Liu, B. Hamamelis-like K₂Ti₆O₁₃ Synthesized by Alkali Treatment of Ti₃C₂ MXene: Catalysis for Hydrogen Storage in MgH₂. *ACS Sust. Chem. Eng.* **2020**, *8*, 4755–4763. [[CrossRef](#)]
42. Wang, Z.Y.; Zhang, X.L.; Ren, Z.H.; Liu, Y.; Hu, J.J.; Li, H.W.; Gao, M.X.; Pan, H.G.; Liu, Y.F. In situ formed ultrafine NbTi nanocrystals from a NbTiC solid-solution MXene for hydrogen storage in MgH₂. *J. Mater. Chem. A* **2019**, *7*, 14244–14252. [[CrossRef](#)]
43. Liu, Y.; Gao, H.; Zhu, Y.; Li, S.; Zhang, J.; Li, L. Excellent catalytic activity of a two-dimensional Nb₄C₃T_x (MXene) on hydrogen storage of MgH₂. *Appl. Surf. Sci.* **2019**, *493*, 431–440. [[CrossRef](#)]
44. Li, J.X.; Wang, S.; Du, Y.L.; Liao, W.H. Catalytic effect of Ti₂C MXene on the dehydrogenation of MgH₂. *Int. J. Hydrogen Energy* **2019**, *44*, 6787–6794. [[CrossRef](#)]
45. Gao, H.; Liu, Y.; Zhu, Y.; Zhang, J.; Li, L. Catalytic Effect of Sandwich-Like Ti₃C₂/TiO₂(A)-C on Hydrogen Storage Performance of MgH₂. *Nanotechnology* **2019**, *31*, 115404. [[CrossRef](#)]

46. Shen, Z.; Wang, Z.; Zhang, M.; Gao, M.; Hu, J.; Du, F.; Liu, Y.; Pan, H. A novel solid-solution MXene ($\text{Ti}_{0.5}\text{V}_{0.5}$) $_3\text{C}_2$ with high catalytic activity for hydrogen storage in MgH_2 . *Materialia* **2018**, *1*, 114–120. [[CrossRef](#)]
47. Liu, Y.; Du, H.; Zhang, X.; Yang, Y.; Gao, M.; Pan, H. Superior catalytic activity derived from a two-dimensional Ti_3C_2 precursor towards the hydrogen storage reaction of magnesium hydride. *Chem. Commun.* **2016**, *52*, 705–708. [[CrossRef](#)]

Disclaimer/Publisher's Note: The statements, opinions and data contained in all publications are solely those of the individual author(s) and contributor(s) and not of MDPI and/or the editor(s). MDPI and/or the editor(s) disclaim responsibility for any injury to people or property resulting from any ideas, methods, instructions or products referred to in the content.